Streamwise and spanwise plasma actuators for flow-induced cavity noise control

Xun Huang and Xin Zhang
Aeronautics and Astronautics, School of Engineering Sciences, University of Southampton, Southampton SO17 1BJ, United Kingdom

(Received 15 December 2007; accepted 6 February 2008; published online 12 March 2008)

Plasma actuators operating in atmospheric air can induce a body force through collisions between electrically charged particles and neutral air molecules by an externally applied electric field. The fast response and the simple structure make the plasma actuator a promising option in aerospace applications. In this work, experiments were performed with several alternative current excited plasma (streamwise and spanwise) actuators to control flow-induced noise from a cavity. It was found that the streamwise actuator induced three-dimensional variations in the shear layer. The spanwise actuator, however, has little influence on the global flow field. As a result, the streamwise actuator is more effective than the spanwise actuator in cavity noise attenuation. © *2008 American Institute of Physics*. [DOI: 10.1063/1.2890448]

I. INTRODUCTION

There is a significant environmental impact on the communities near airports imposed by flow-induced noise generated by the takeoff and approach to landing of aircraft,[1] during which stages a large portion of aircraft noise is contributed from airframe due to the advent of low-noise aeroengines with high bypass ducts. The airframe noise comes from high lift devices, landing gear, wheel wells, and sharp trailing edges. It is particularly evident in the stage of approach to landing when aeroengines are at a low power setting with the high lift devices and landing gear deployed. Active flow control using plasma actuators operating in atmospheric pressure air[2] holds the potential to reduce flow-induced noise that may be helpful to meet the reduction target of perceived noise level of 50% by 2020.[3]

Although noise reduction solutions exist in the form of liners, porous materials, and various aerodynamic devices, it is apparent that the passive solutions fail to work at off-design conditions. The demand for active aeroacoustic control solutions has encouraged the investigation of various actuators to enhance aerodynamic performance. Nevertheless, active devices such as piezoelectric actuators and blowing/suction jets pose installation and maintenance issues. In contrast, plasma actuators are simple and cheap to manufacture and install. The simplicity and absence of any mechanical moving parts, for example, pump or blowing/suction slots, make plasma actuators quite promising alternatives for aerospace applications.

The principle of using plasma for flow control is not new. The history was already summarized by Moreau.[4] The recent invention by Roth[2] that can produce sufficient quantities of glow discharge plasma in the atmosphere pressure air helps to yield an increase in flow control performance. Although the precise flow control physics under plasma actuation is still far from being understood clearly and more research needs to be performed, it is evident that the flow local to plasma actuators on an aerodynamic surface is altered, leading to global changes in the surrounding flow field. This method offers possibilities to noise control (without the need to physically change the shape of the aerodynamic surface) as flow and surface interaction represents one of the dominant sources of aerodynamic noise.

Two mechanisms affect the flow field local to plasma actuators by electric discharges. The first one is the local heating of the airflow caused by arc filaments[5] or direct current discharges:[6,7] Heat energy is added to the surrounding airflow leading to an increase of the local sound speed and a reduction of gas density. The second one is to manipulate the surrounding airflow by an externally applied electric field: momentum is transferred from the charged particles to the neutral gas through collisions between oxygen/nitrogen plasma components and neutral air molecules.[2,4]

The plasma actuators employed in this work belong to the second type. Our study seeks to understand noise attenuation physics through the experimental investigation of the local flow field and the sound pressure level (SPL) reduction. Plasma actuators with two different geometrical structures were used to control flow-induced noise of a cavity that is similar to landing gear and weapon bay. The experimental setup is given in Sec. II. The relevant electric, aerodynamic, and acoustic results are discussed in Sec. III. A brief summary is provided in the end of this paper.

II. EXPERIMENTAL SETUP

A. Plasma actuators

Figure 1 shows the geometries of two plasma actuators that were developed in this work. The actuators were implemented on 350×150 mm^2 printed circuit boards (PCBs). The geometries were selected empirically to increase flow control performance for the investigated test case. The dielectric material between electrodes is flame retardant 4. The depth of the dielectric material is 1.27 mm. In Figs. 1(a) and 1(b), the sections of electrodes that generate discharges are perpendicular to the oncoming mean flow and span the di-

 © 2008 American Institute of Physics

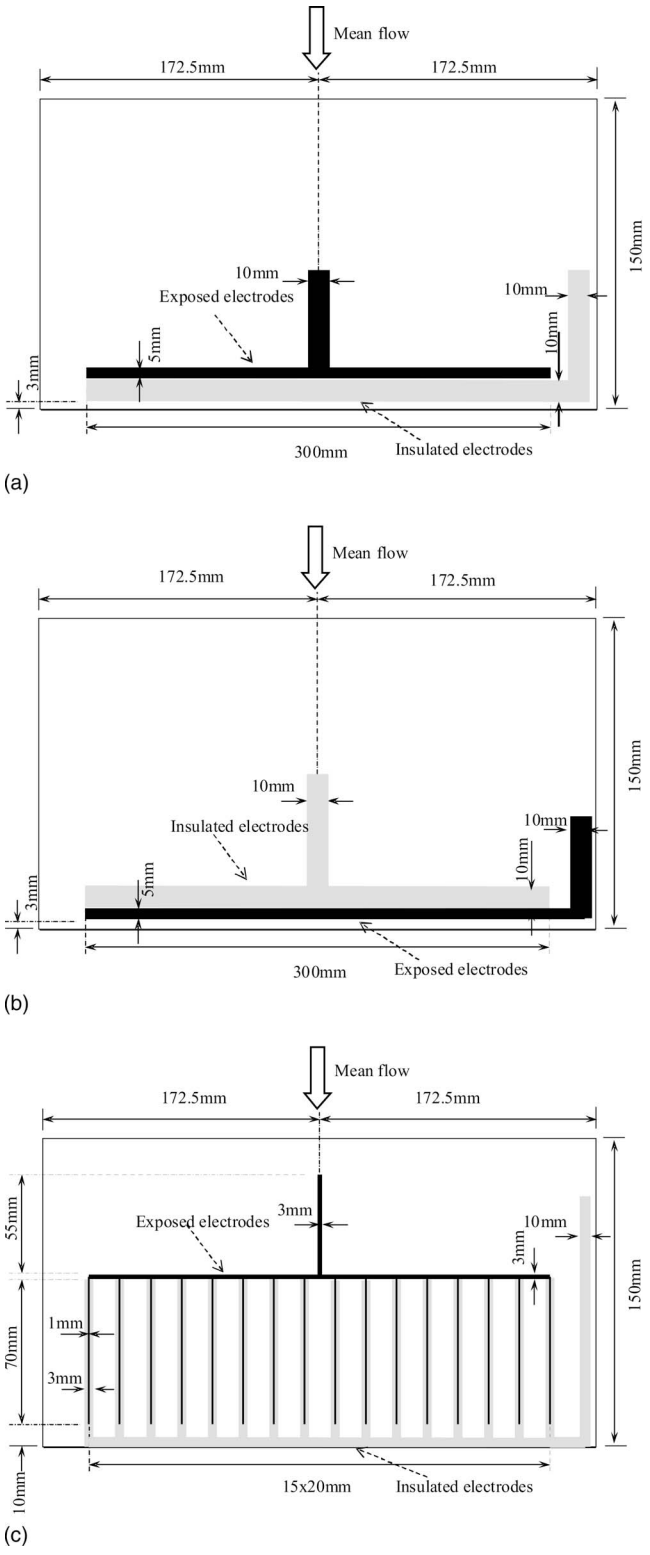

FIG. 1. Schematics of plasma actuators (not to scale): (a) The spanwise actuator that generates downstream actuation, (b) the spanwise actuator that generates upstream actuation, and (c) the streamwise actuator that generates spanwise actuation, where the black lines represent exposed electrodes and the gray lines represent insulated electrodes.

electric board. According to the layouts, they are called as spanwise actuators in the rest of the paper. In addition, to avoid bottom surface discharges that are useless to manipulate airflow, the bottom electrodes are insulated by dielectric

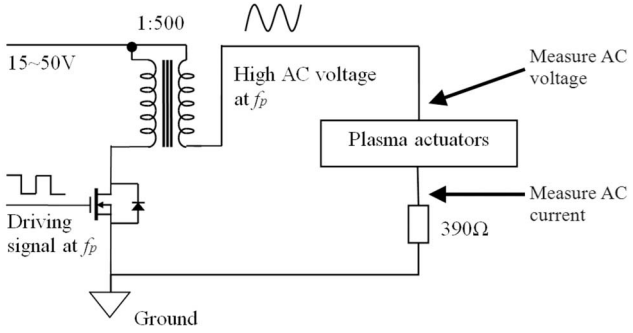

FIG. 2. Schematic of the electric setup.

materials. Otherwise, the system power efficiency will be sacrificed. As determined by the positions of the electrodes, the plasma actuator displayed in Fig. 1(a) generates body force in the downstream direction; the plasma actuator displayed in Fig. 1(b) produces body force in the upstream direction. The spanwise length of the exposed electrode is 300 mm; the spanwise length of the insulated electrodes is 320 mm. The width is 10 mm for insulated electrodes and 5 mm for exposed electrodes. The streamwise gap between exposed and insulated electrodes is 0 mm.

In Fig. 1(c), the major sections of electrodes generating discharges are aligned with the oncoming mean flow. The actuator is therefore called as a streamwise actuator in the rest of the paper. The spanwise gap between the consecutively exposed electrodes is 14 mm; the spanwise gap between the consecutively insulated electrodes is 12 mm. The center lines of both exposed electrodes and insulated electrodes are aligned. The width of the exposed electrodes is 1 mm; the width of the insulated electrodes is 3 mm. The geometries were selected empirically to improve the actuator performance. More detailed discussions about the optimization of geometries in terms of the aerodynamic performance can be found in literatures.[8–10]

B. Electric components

To generate atmospheric glow discharges in air, a sufficiently high electric field is required to break down the air species local to high voltage electrodes. The voltage applied to the electrodes operates at O(kHz) frequency to sustain the glow discharge. Rather than using a linear power amplifier, which was employed previously,[11,12] the power supply used in our studies employs a simple switching circuit topology (see Fig. 2) that restricts the driving signal to square wave. Electron avalanches that lead to arcing are prevented by the dielectric material (barrier) between exposed electrodes and insulated electrodes. The exposed electrodes on the flow facing surface are connected to the high voltage power supply that is of sinusoidal form. The insulated electrodes are grounded. The converse setup is more insensitive to humidity but generates less actuation due to the weaker electric field above the flow facing surface. The optimal driving frequency (f_p) for a specific plasma actuator can be determined in terms of the noise attenuation effect. For the present plasma actuators, the value of f_p ranges from 3 to 6 kHz that

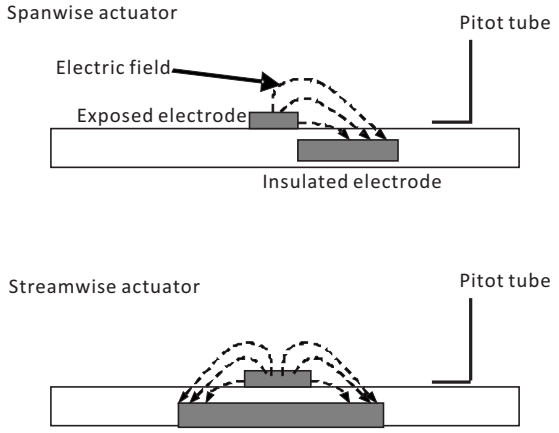

FIG. 3. Schematic of the induced velocity measurement setup.

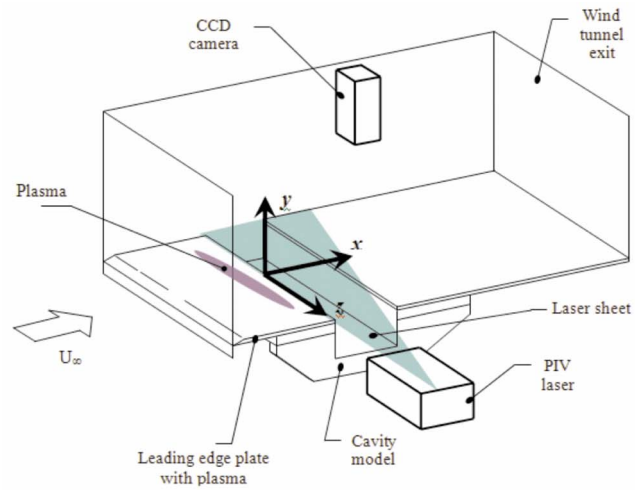

FIG. 4. (Color online) PIV measurement setup for (a) plan-view and (b) side-view measurements.

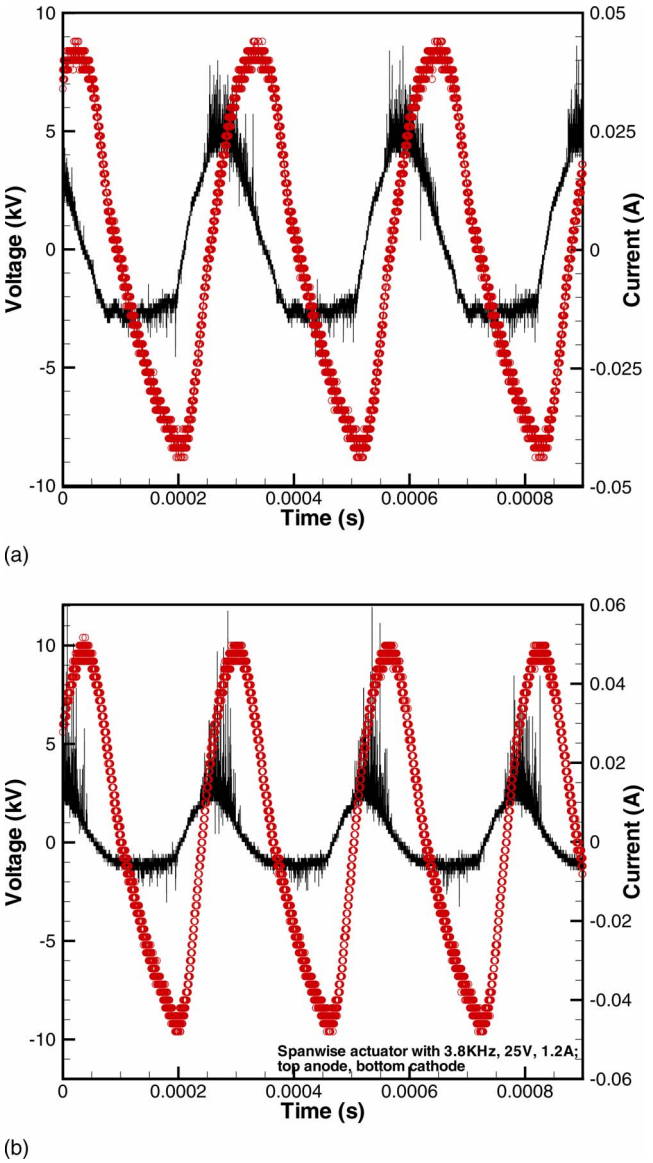

FIG. 5. (Color online) Voltage and current waveforms of (a) the streamwise actuator that operates at f_p=3.2 kHz and (b) the spanwise actuator that operates at f_p=5 kHz, where (○) denotes the voltage waveforms and (—) represents the current waveforms.

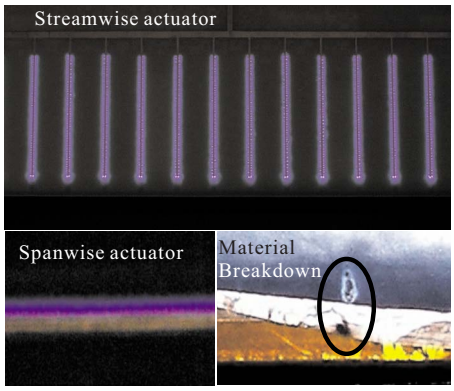

FIG. 6. (Color online) Plasma discharges and the dielectric material failure at quite high voltage.

switches a step up transformer through a power metal-oxide-semiconductor field-effect transistor. Sufficiently high alternating current (ac) supply is subsequently output from the step up transformer to induce discharges. Using impedance matching networks not employed here, the driving frequency f_p can be increased beyond 20 kHz to reduce audible noise radiating from the plasma actuators. More detailed discussion about the driving signal can be found in the literature.[13]

To indicate the operating mode of plasma discharges, the voltage and current waveforms applied to plasma actuators were measured. The externally applied ac voltage was measured directly by a high voltage probe (Testec HVP-15HF). The current through the plasma actuator was measured using the resistive technique with a 390 Ω resistor in series with the plasma actuator, placed between the ground and the plasma actuator. The relevant potential drop on the current measurement resistor is less than 100 V, which is much smaller than the externally applied high voltage (generally the peak-to-peak voltage $V_{\text{p.p.}} > 8$ kV), thus minimally affecting the discharge behavior and the actuator performance. The other two general current measurement techniques using Hall-effect sensors and current transformers are more convenient, but they are also much more expensive and therefore were not considered in this work.

C. Flow testing facilities

In the stationary mean flow environment, the average airflow velocity induced by the plasma actuators was measured using an inexpensive Pitot tube that connects to a Furness FC02 micromanometer. The outer diameter of the Pitot tube tip is 2.3 mm. The inner diameter is 1.5 mm. The measurement error of the micromanometer is within 1%. The measurement position is shown in Fig. 3, where two different perspectives of the plasma actuators were used to display the setup clearly. The orientation of the Pitot tube tip is normal to an exposed electrode. The height between the dielectric surface and the axis of the Pitot tube is 2 mm to obtain the maximal value of the induced velocity. The distance between the exposed electrode and the steel tip is 20 mm. Quite strong interaction with electric field appears when the distance is less than 10 mm, leading to arching between the exposed electrodes and the steel tip. The distance of 20 mm is safe to prevent arching in velocity measurements for the current actuators. It is also worth noting that hot wire anemometer or laser Doppler velocimetry has to be used for studying transient characteristics.

Flow-induced noise control experiments were conducted in a wind tunnel facility at the University of Southampton. The wind tunnel is of a closed jet and open loop design. The working section has a uniform cross section that measures 0.260×0.345 m^2 and has a length of 0.850 m. A cavity model (Fig. 4) manufactured from Perspex was used in experiments to assess the control performance of plasma actuators. The leading edge plate of the cavity was formed by the PCB, on which either the streamwise plasma actuator or the spanwise plasma actuator was etched. The length L of the cavity is 50 mm. The length-to-depth ratio is 1. Although the results presented in the rest of the paper were obtained at the flow speed of 20 m/s, corresponding to a Reynolds number of 7.2×10^4, similar results were also obtained at lower velocities. Unsteady surface pressure of the cavity was measured using a Panasonic WM-60A omnidirectional condenser microphone. The diameter is 6 mm. The lowest sensitive frequency is 20 Hz and the highest one is 20 kHz. The sensitivity is -44 ± 5 dB (0 dB=1 V/Pa at 1 kHz). The signal-to-noise ratio is more than 58 dB. The microphone was flush mounted to the surface of the cavity's front wall. The height of the installation position to the cavity's bottom wall is 25 mm. The microphone's signal was passed through preamplifier and antialiasing filter and subsequently sampled with a personal computer's sound card at 44.1 kHz. The electric circuits were shielded to prevent electromagnetic interference from discharges. A 4096 point fast Fourier transform with a Hanning window function was applied to the sampled data. The spectral results were averaged over 300 signal blocks for statistical confidence.

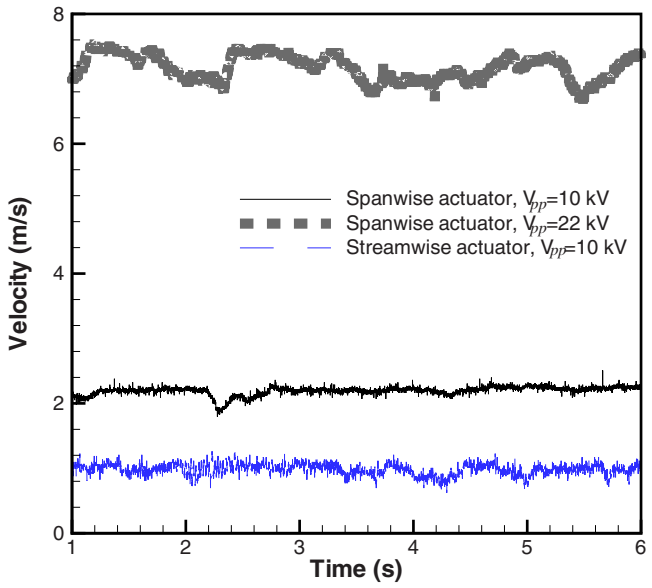

FIG. 7. (Color online) Airflow velocity induced by the plasma actuators.

The influence of the electric discharge on the local flow field was investigated using a particle image velocimetry (PIV) system that measures two-dimensional velocity field. The PIV system used in the experiments was produced by Dantec Measurement Systems and incorporates two Gemini neodymium-doped yttrium aluminium garnet (Nd:YAG) lasers by NewWave Research that are capable of running at 16 Hz double-pulse repetition rate, emitting pulses at 532 nm light frequency to illuminate seeding particles, which are provided to represent the flow using a Safex S195G smoke seeder by Marin Professional. The typical sizes of the nonspherical particles are 2 μm in diameter. The particles provide suitable tracer material that is homogeneously distributed into the flow. A Dantec HiSense (type 13 gain 4) 1024×1289 resolution charge-coupled device camera was operated in a double frame mode (2 Hz) to capture digital images of the flow field on the plan-view domain [Fig. 4(a)] and side-view domain [Fig. 4(b)]. The coordinates employed throughout the paper were also displayed in Fig. 4,

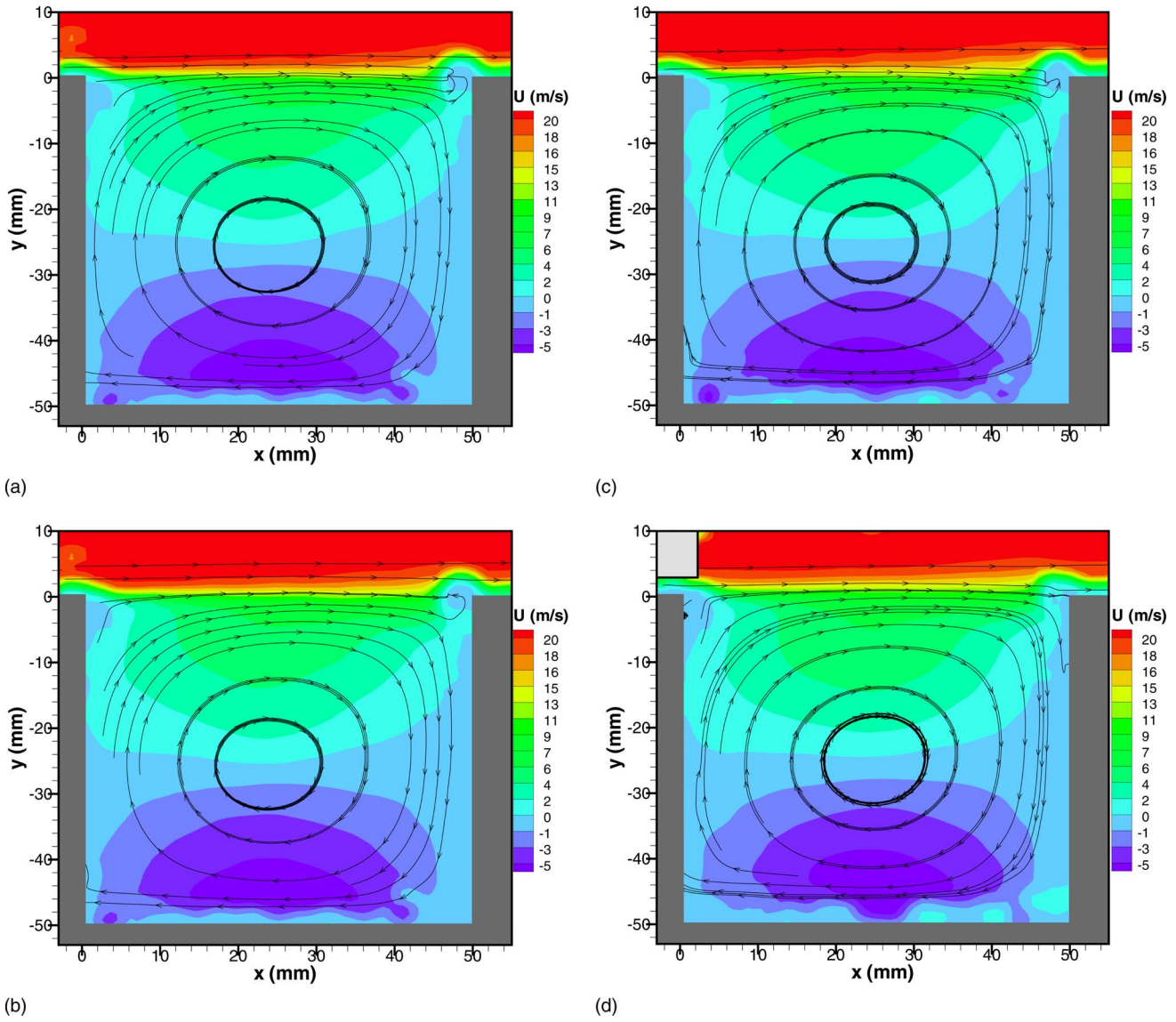

FIG. 8. (Color online) Mean velocity U (in the x direction) and the streamlines under (a) inactive actuation, (b) downstream actuation, (c) upstream actuation, and (d) spanwise actuation, where $U_\infty = 20$ m/s and $V_{\text{p.p.}} = 15$ kV.

where the x coordinate is at the center of the cavity's leading wall. For each experiment, 250 images of the flow field were taken for the postprocessing, in which the velocity was calculated by performing time-domain analysis (cross-correlation technique) on the successive images.

III. RESULTS AND DISCUSSION

A. Electric properties

As shown in Fig. 5, the voltage and current waveforms are similar for both the spanwise actuator and the streamwise actuator. Almost 90° of the phase lag between the voltage waveform and the current waveform indicates that the plasma produced is capacitively coupled. As the bottom electrodes are insulated and most discharges appear on the flow facing surface, the current waveforms are asymmetrical. The current waveforms also suggest that the operating mode of the plasma actuators is the combination of glow discharge and filamentary discharge.[14] The latter one consists of numerous microdischarges that are collected by the exposed electrode to form the current peaks. The filaments from the streamwise actuator, as displayed in Fig. 6, for example, could be observed clearly by the naked eye.

B. Induced velocities

The induced airflow velocities local to the actuators are shown in Fig. 7, where the results were measured in an environment with stationary mean flow. The results indicate that the collective body force generated by the momentum transfer between charged particles and neutral components is from the exposed electrodes to the insulated electrodes. In addition, the spanwise actuator induces higher voltage than the streamwise actuator does. The difference at $V_{\text{p.p.}} = 10$ kV was mainly caused by the geometries: The collective length of electrodes that generate plasma is 2100 mm for the streamwise actuator, much longer than the 300 mm length of

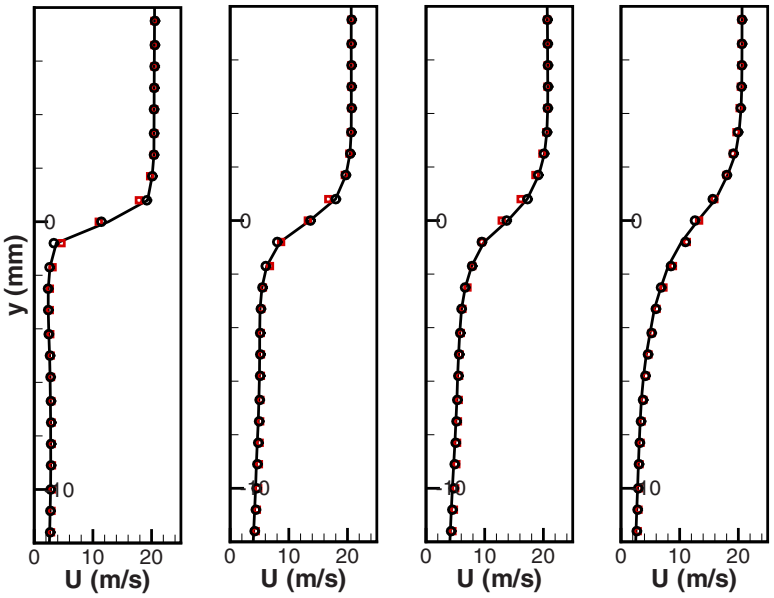

FIG. 9. (Color online) U profiles at four side-view positions, where $z=0$ mm, and x coordinates are, from left to right, 10, 20, 30, and 40 mm. The results were obtained when (—) the spanwise plasma actuator is inactive, (○) the spanwise plasma actuator generates upstream actuation, and (□) the spanwise plasma actuator provides downstream actuation.

the working section for the spanwise actuator. Compared with the spanwise actuator, less power is distributed to each unit of the streamwise actuator. The induced velocity from the spanwise actuator is therefore higher.

The induced airflow velocity could be increased if a higher $V_{\text{p.p.}}$ is applied to the plasma actuators. The maximal velocity achieved in our laboratory is 7.8 m/s when $V_{\text{p.p.}}$ is 22 kV. Once $V_{\text{p.p.}}>22$ kV, the dielectric material will be broken down. Figure 6 gives an example of the dielectric material failure with $V_{\text{p.p.}}=26$ kV. The sustainable voltage could be increased by increasing the thickness of the dielectric material. The treatment increases the electric impedance of the actuators, leading less power to the desirable discharges, and fails to induce higher velocity. Up to now, the maximal velocity produced by glow discharge/dielectric barrier discharge is below 8 m/s.[2,4,9,10] The relatively low authority of a plasma actuator remains a great concern for high speed flow control applications. To solve the problem, both new dielectric materials with high dielectric strength/constant and intelligent control method that applies plasma actuation more efficiently[15] have to be studied. The investigation on the two topics is ongoing and beyond the scope of this paper.

C. PIV results

The mean velocity U in the x direction is compared in Fig. 8, where the free stream velocity $U_\infty=20$ m/s and $V_{\text{p.p.}}=15$ kV. The cavity wall is represented by several deep gray colored blocks. The laser sheet of PIV is located at $z=10$ mm, which coincides with one electrode of the streamwise plasma actuator [see Fig. 4(b)]. The imperfection of the captured image in Fig. 8(d) is caused by the bright plasma. It is excluded by a light gray colored block. Figure 8 shows that the mean flow fields with/without plasma actuation have quite similar patterns.

To show the difference in the previous PIV results more clearly, Figs. 9 and 10 compare the U profiles at four positions, under inactive actuation, upstream actuation, downstream actuation, and spanwise actuation. Figure 9 shows that the U profile under either upstream actuation or downstream actuation closely resembles the U profile without plasma actuation, indicating that the spanwise plasma actuator has little influence on the global flow field.

For the streamwise plasma actuator, the U profiles were measured at two x-y planes with $z=0$ and 10 mm. The former one is between two consecutive electrodes in the center of Fig. 1(c). The latter one coincides with the exposed electrode at $z=10$ mm [see Fig. 1(c)]. Figure 10 shows that the streamwise plasma actuator is capable of influencing the flow field, even at 50 mm away from the actuator. Compared with under inactive actuation, by using spanwise actuation, velocity U in the shear layer is reduced slightly at $z=0$ mm; on the other hand, velocity U in the shear layer is increased at $z=10$ mm. The results indicate that the streamwise plasma actuator generates spanwise variance in the U profile.

To show the spanwise variance more clearly, the laser sheet was set to $y=0$ to visualize the two-dimensional flow field right over the cavity [see Fig. 4(a)]. The plan-view PIV results are shown in Fig. 11. Figure 11(a) shows that the velocity U distribution is approximately uniform across the z coordinate when the streamwise plasma actuator is inactive. In contrast, Fig. 11(b) shows the variance in the z direction distinctively. Each velocity variance coincides with one electrode of the streamwise actuator. In other words, there is a three-dimensional variation introduced by the streamwise actuator.

Galilean decomposition[16] was performed on the instantaneous velocity vectors to visualize vortical structures. The convective velocity U_c of the vortices in the shear layer was set to $0.6U_\infty$,[17] based on which the Galilean analysis produced images with clear vortical structures in the shear layer.

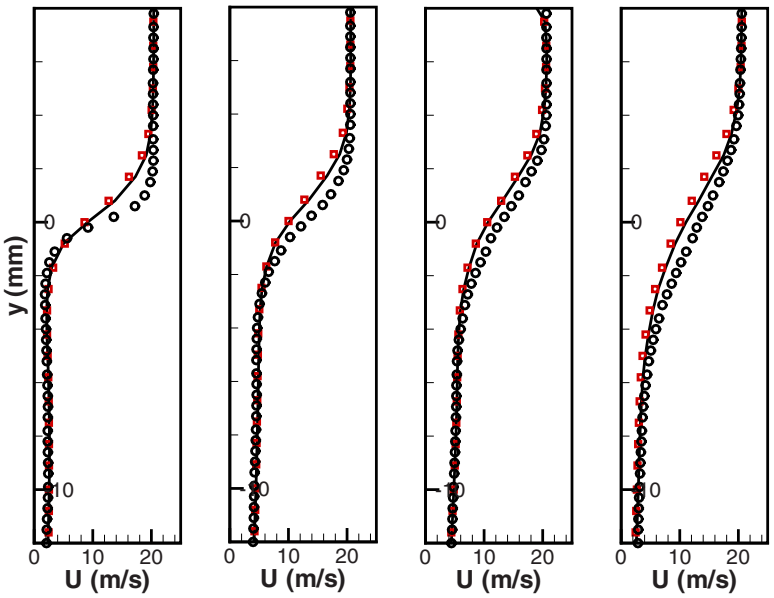

FIG. 10. (Color online) U profiles at four side-view positions, where x coordinates are, from left to right, 10, 20, 30, and 40 mm. The results were obtained when (-) the streamwise plasma actuator is inactive and $z=0$ mm, (○) the streamwise plasma actuator is active and $z=10$ mm, and (□) the streamwise plasma actuator is active and $z=0$ mm.

When the plasma actuators are inactive, the vortical structures originate from the leading edge of the cavity, develop in the shear layer, and impinge on the trailing edge of the cavity. One instantaneous result is displayed in Fig. 12(a). When the spanwise actuator is active to generate either upstream actuation or downstream actuation, the length scales and vortical structures are still similar to the case without plasma actuation. Two instantaneous results at approximately the same time are displayed in Figs. 12(b) and 12(c). In contrast, when using the streamwise actuator to produce spanwise actuation, the length scale of the vortical structures is increased in almost half samples at $z=10$ mm [see Fig. 12(d)]; the large-scale vortical structures are absent in other images measured at the same place [see Fig. 12(e)]. The intermittence of discrete vortices under spanwise actuation was already discussed in our previous work.[18] In this work, we also investigated the flow field at $z=0$ mm, where the large-scale vortical structures were found to be absent in the shear layer in almost all images [see Fig. 12(f)]. Moreover, compared with Fig. 12(a), the variances of length scale in Figs. 12(d)–12(f) reflect the fact that the instantaneous velocity U is larger at $z=10$ mm, and smaller at $z=0$ mm. The instantaneous flow discovery is consistent with the mean flow results displayed in Figs. 10 and 11.

D. Acoustic results

The performance of the actuators on the noise attenuation is compared in Fig. 13, where the mean flow velocity U_∞ is 20 m/s and $V_{\text{p.p.}}=15$ kV. The tonal noise at approximately 300 Hz is caused by the wind tunnel fan noise that cannot be affected by plasma actuators. In addition, other than attenuating flow-induced tones, the plasma actuators also produce high frequency acoustic tones and electromagnetic radiations at the plasma driving frequency f_p, which is 5 kHz for the spanwise actuator and is 3.2 kHz for the streamwise actuator.

Figure 13(a) shows that the SPL magnitude at the dominant frequency was reduced by 12 dB under the downstream

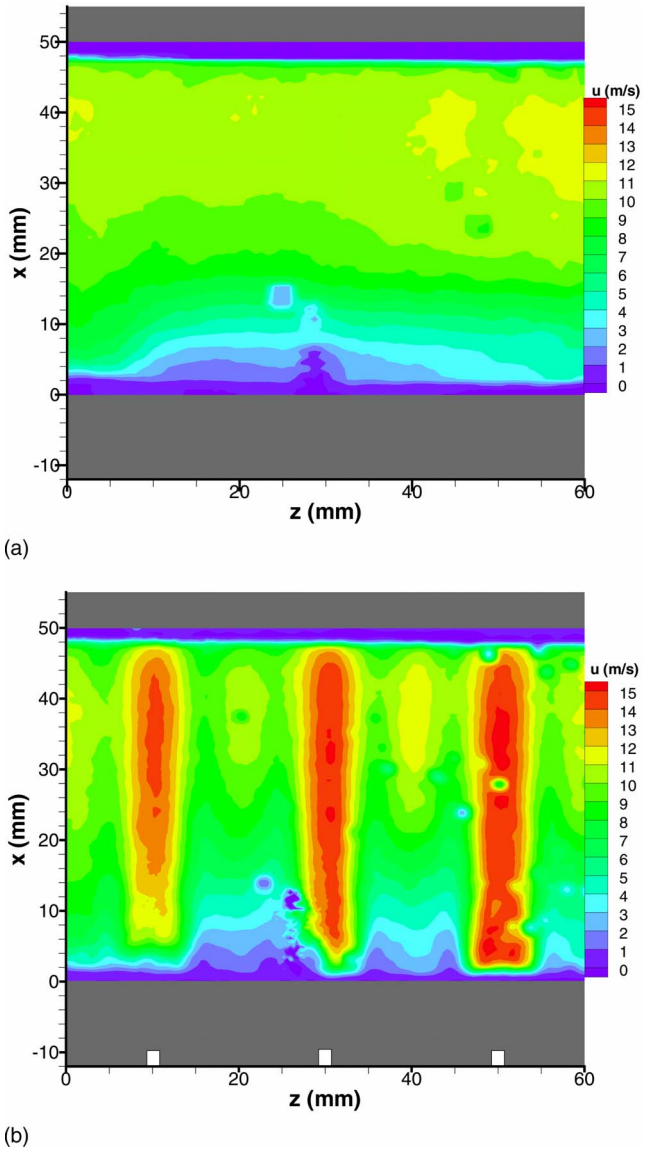

FIG. 11. (Color online) Mean velocity U (in the x direction) spanning the cavity, where $y=0$ mm, U_∞ is from bottom to top, and the streamwise plasma actuator (a) is inactive and (b) is active.

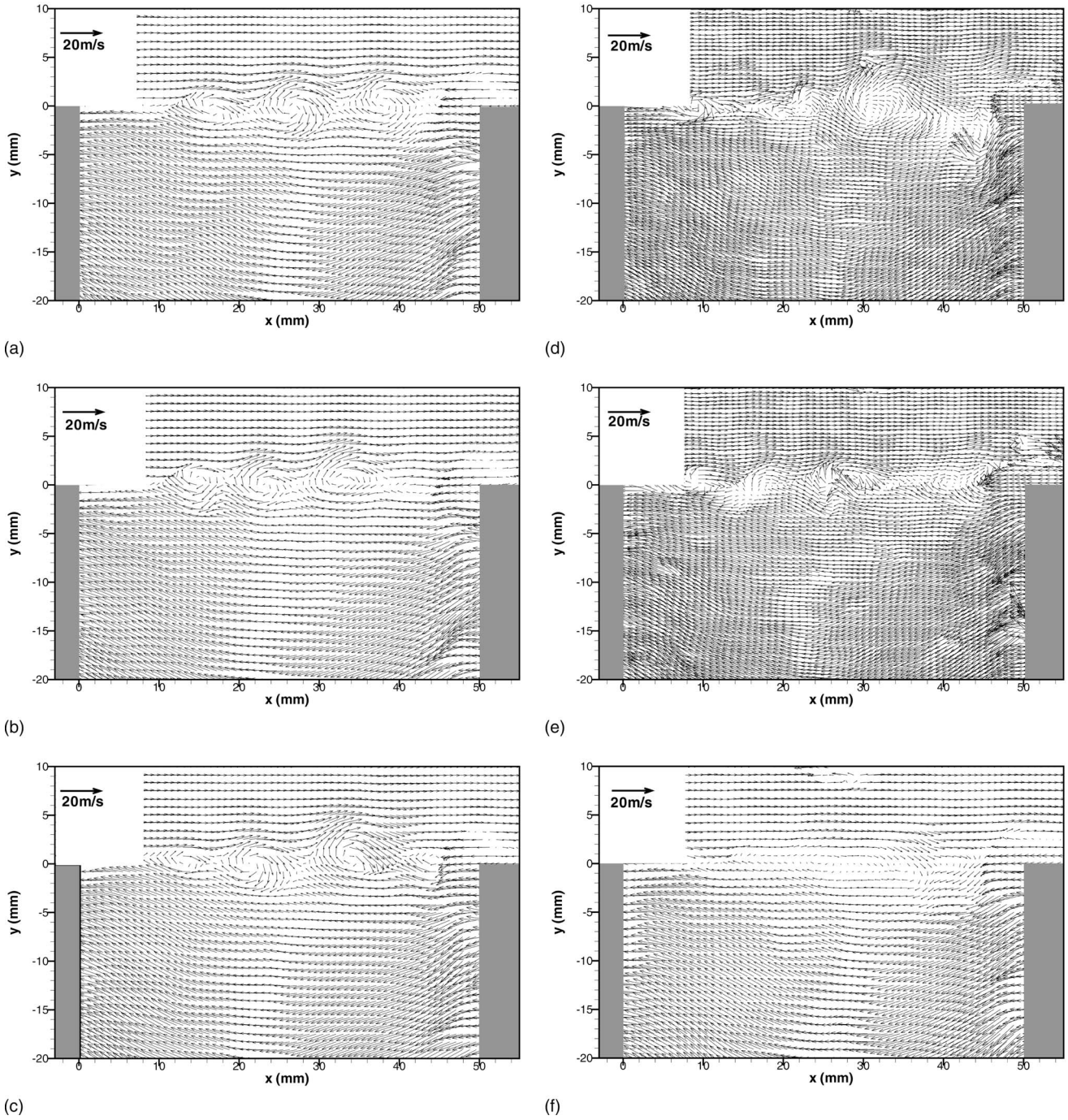

FIG. 12. Instantaneous vortical structures in the shear layer, when (a) the plasma actuators are inactive, (b) the spanwise actuator is active to produce downstream actuation, (c) the spanwise actuator is active to produce upstream actuation, (d) the streamwise actuator is active to produce spanwise actuation (measured at $z=10$ mm), (e) is the same as (d) but at a different moment, and (f) is the same as (d) but measured at $z=0$ mm.

actuation. On the other hand, Fig. 13(b) shows that the SPL magnitude at the dominant frequency was reduced by 16 dB under the upstream actuation. The SPL magnitudes at the other frequencies range from 400 to 1100 Hz, however, were increased by 1–3 dB. In contrast to the spanwise actuator, the streamwise actuator attenuated the dominant tonal noise completely. In Fig. 13(c), the magnitude levels at the second and the fifth Rossiter frequencies (422 and 1145 Hz) (Ref. 17) were removed entirely; the magnitude level at the third Rossiter frequency (663 Hz) was reduced by 3 dB. The nth Rossiter frequencies f_R were computed by an empirical formula $f_R=U_\infty(n-\gamma)/[L(M_\infty+1/\kappa)]$, where $\gamma=0.25$, $\kappa=0.625$,[17] $M_\infty=U_\infty/C$, C is the sound speed, and L is the cavity length. In addition, the remaining tonal noise at the third Rossiter frequency can be attenuated completely by increasing the system power to 60 W. It is also worth noting that the SPL results in Fig. 13 mainly reflect the near field unsteady pressure attenuation; the difference in driving frequencies (5 and 3.2 kHz) is caused by the different impedances of the plasma actuators.

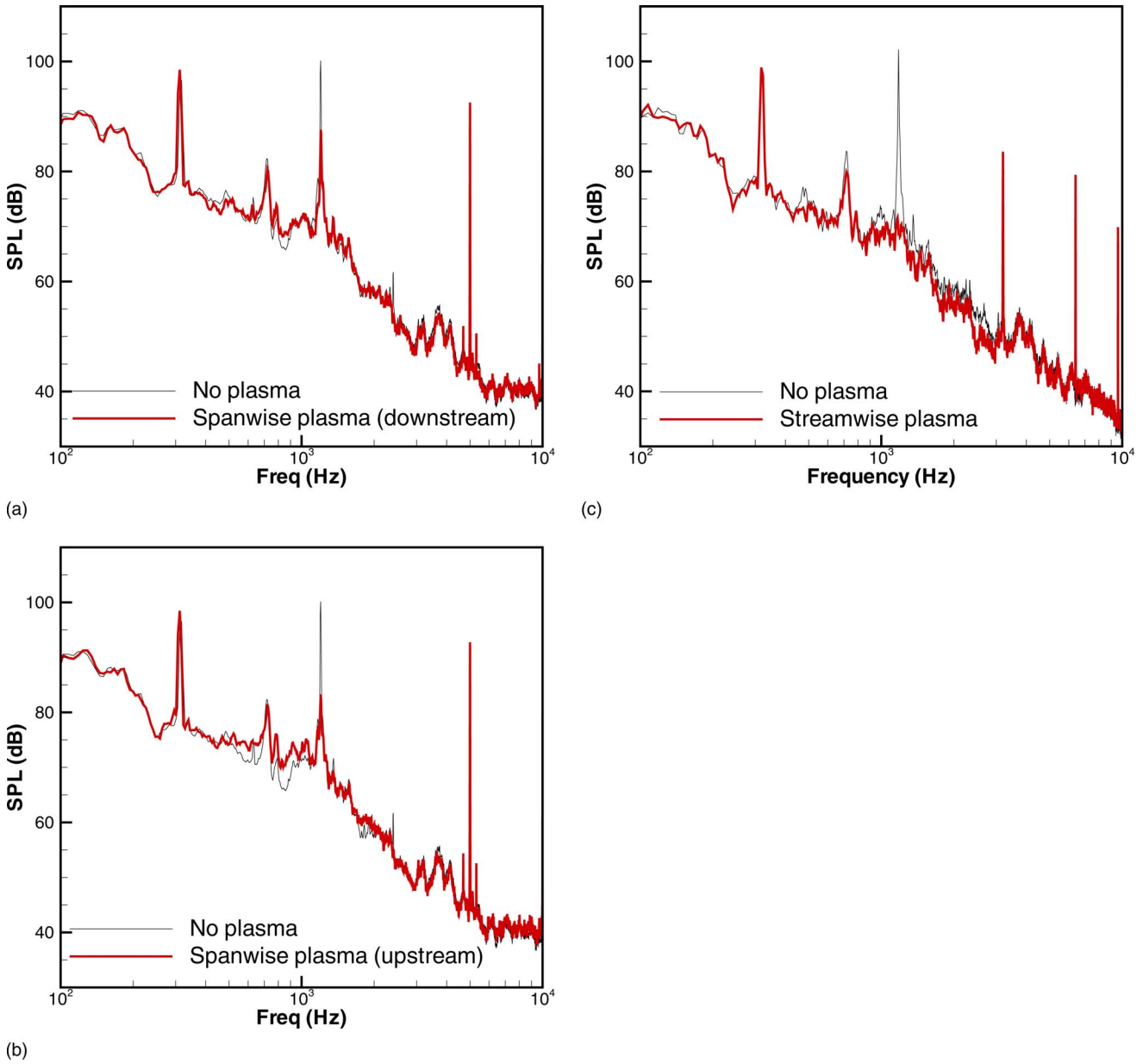

FIG. 13. (Color online) Sound level reduction at $U_\infty = 20$ m/s by using (a) the spanwise plasma actuator with downstream actuation, (b) the spanwise plasma actuator with upstream actuation, and (c) the streamwise plasma actuator with spanwise actuation, where $V_{\text{p.p.}} = 15$ kV, f_p is 5 kHZ for the spanwise actuator, and 3.2 kHz for the streamwise actuator.

E. Discussion

Several possible active flow control mechanisms in cavity noise attenuation were already summarized in the literature,[19] which include the following: Affecting the boundary layer/shear layer thickness to change hydrodynamic stability characteristics, introducing disturbances at off-resonant frequencies to impede the natural resonance, and shifting the reattachment location of the shear layer on the cavity's trailing wall to interrupt/reduce the acoustic feedback. The PIV results in Figs. 8–13 show that the spanwise actuator with either upstream actuation or downstream actuation affects little on the shear layer spanning the cavity. The velocity fluctuation driven by the spanwise actuator, however, is at the frequency f_p (5 kHz) that is much higher than the dominant resonance frequency (1145 Hz) of the cavity. The disturbances introduced by the spanwise actuator could therefore attenuate the resonance at the dominant frequency through nonlinear interactions.[19] On the other hand, the streamwise actuator cannot only provide the actuation at an off-resonant frequency (3.2 kHz) but also manipulate the shear layer extensively. Figure 10 shows that the local shear layer thickness is reduced at $z = 10$ mm and is increased at $z = 0$ mm. The vortical thickness $\delta_\omega = (U_{\max} - U_{\min})/(\partial U/\partial y)|_{\max}$ is taken to be the local shear layer thickness. The disturbances are consequently amplified in the shear layer at different rates and, more importantly, at differ-

ent phases that can offset each other. The collective result is the complete attenuation of the tonal noise at the dominant frequency.

IV. SUMMARY

The aim of this experimental investigation was to investigate the noise control effects of the spanwise actuator and the streamwise actuator. The measured electric properties revealed that the operating mode of the plasma actuators is the combination of glow discharge and filamentary discharge. For the current setup, the maximal induced velocity achieved in our laboratory is approximately 8 m/s. The plasma actuators were applied to the cavity at $U_\infty = 20$ m/s to investigate the noise attenuation effect. Both microphone measurements within the cavity and PIV surveys for the cavity flow were performed. PIV results show that the spanwise actuators affect the shear layer little. In contrast, the streamwise actuator can produce the spanwise actuation that manipulates the flow field in the z direction. The acoustic measurements show that both the spanwise actuators and the streamwise actuator can attenuate the dominant tonal noise by more than 12 dB. However, the attenuation mechanisms are different: the spanwise actuator drives the flow at off-resonant frequency. In addition to that, the streamwise actuator can modify hydrodynamic stability characteristics through manipulating the shear layer in three-dimensional domain. The streamwise actuator was found to be more effective in cavity tonal noise attenuation.

Compared with other alternatives, the plasma actuators have a lot of merits, which include the following: the implementation of the plasma actuator is simple and cheap; the overall system weight can be light; the plasma actuators can be installed on aircraft structure surface directly and thus impose little effect on overall structure; the plasma actuators have rapid time response. In summary, the method of using atmospheric pressure plasma actuators is quite promising in flow control applications.

ACKNOWLEDGMENTS

The authors would like to thank Dr. Sammie Chan for fruitful discussions and help on the experimental setting.

[1] G. Raman and D. K. McLaughlin, "Recent aeroacoustics research in the United States," Noise Vib. Control Worldw. **31**, 15 (2000).
[2] J. R. Roth, D. M. Sherman, and S. P. Wilkinson, "Electrohydrodynamic flow control with a glow-discharge surface plasma," AIAA J. **38**, 1166 (2000).
[3] Advisory Council for Aeronautics Research in Europe, "Strategic research agenda," Strategic research agenda 1–2 (2002).
[4] E. Moreau, "Airflow control by non-thermal plasma actuators," J. Phys. D **40**, 605 (2007).
[5] Y. G. Utkin, S. Keshav, J. H. Kim, J. Kastner, I. V. Adamovich, and M. Samimy, "Development and use of localized arc filament plasma actuators for high-speed flow control," J. Phys. D **40**, 685 (2007).
[6] S. El-Khabiry and G. Colver, "Drag reduction by DC corona discharge along and electrically conductive flat plate for small Reynolds number flow," Phys. Fluids **9**, 587 (1997).
[7] E. Moreau, L. Léger, and G. Touchard, "Effect of a DC surface non-thermal plasma on a flat plate boundary layer for airflow velocity up to 25 m/s," J. Electrost. **64**, 215 (2006).
[8] C. L. Enloe, T. E. McLaughlin, R. D. Van Dyken, K. D. Kachner, E. J. Jumper, T. C. Corke, M. Post, and O. Haddad, "Mechanisms and responses of a dielectric barrier plasma actuator: Geometric effects," AIAA J. **42**, 595 (2004).
[9] J. R. Roth and X. Dai, "Optimization of the aerodynamic plasma actuator as an electrohydrodynamic (EHD) electrical Device," AIAA Paper No. 2006–1203, 2006.
[10] M. Forte, J. Jolibois, J. Pons, E. Moreau, G. Touchard, and M. Cazalens, "Optimization of a dielectric barrier discharge actuator by stationary and non-stationary measurements of the induced flow velocity: Application to airflow control," Exp. Fluids **43**, 917 (2007).
[11] C. L. Enloe, T. E. McLaughlin, R. D. Van Dyken, K. D. Kachner, E. J. Jumper, and T. C. Corke, "Mechanisms and responses of a single dielectric barrier plasma actuator: Plasma morphology," AIAA J. **42**, 589 (2004).
[12] J. R. Roth, "Aerodynamic flow acceleration using paraelectric and peristaltic electrohydrodynamic effects of a one atmosphere uniform glow discharge plasma (OAUGDP)," Phys. Plasmas **10**, 2117 (2003).
[13] X. Huang, S. Chan, X. Zhang, and S. Gabriel, "An atmospheric plasma actuator for aeroacoustic applications," IEEE Trans. Plasma Sci. **35**, 693 (2007).
[14] I. Muller, C. Punset, E. Ammelt, H. G. Purwins, and J. P. Boeuf, "Self-organized filaments in dielectric barrier glow discharges," IEEE Trans. Plasma Sci. **27**, 20 (1999).
[15] X. Huang, S. Chan, X. Zhang, and S. Gabriel, "Variable structure model for flow-induced tonal noise control with plasma actuators," AIAA J. **46**, 241 (2008).
[16] R. J. Adrian, K. T. Christensen, and Z. C. Liu, "Analysis and interpretation of instantaneous turbulent velocity fields," Exp. Fluids **29**, 275 (2000).
[17] J. E. Rossiter, "Wind-tunnel experiments on the flow over rectangular cavities at subsonic and transonic speeds," Aeronaut. Res. Counc. Rep. Memo. 3438 (1964).
[18] S. Chan, X. Zhang, and S. Gabriel, "The attenuation of cavity tones using plasma actuators," AIAA J. **45**, 1525 (2007).
[19] C. W. Rowley and D. R. Williams, "Dynamics and control of high-Reynolds-number flow over open cavities," Annu. Rev. Fluid Mech. **38**, 251 (2006).